Journal of Magnetic Resonance 353 (2023) 107515

Contents lists available at ScienceDirect

Journal of Magnetic Resonance

journal homepage: www.elsevier.com/locate/jmr

# The electronic structure and dynamics of the excited triplet state of octaethylaluminum(III)-porphyrin investigated with advanced EPR methods

Angelo Carella [a,1], Susanna Ciuti [a,1], Haakon T.A. Wiedemann [b], Christopher W.M. Kay [b,c], Arthur van der Est [d], Donatella Carbonera [a], Antonio Barbon [a,*], Prashanth K. Poddutoori [e], Marilena Di Valentin [a,*]

[a] Department of Chemical Sciences, University of Padova, Via Marzolo 1, 35131 Padova, Italy
[b] Department of Chemistry, Saarland University, Campus B 2.2, 66123 Saarbrücken, Germany
[c] London Centre for Nanotechnology, University College London, 17-19 Gordon Street, London WC1H 0AH, UK
[d] Department of Chemistry, Brock University, 1812 Sir Isaac Brock Way, St. Catharines, Ontario, Canada
[e] Department of Chemistry & Biochemistry, University of Minnesota Duluth, 1038 University Drive, Duluth, MN 55812, USA

ARTICLE INFO

*Article history:*
Received 21 April 2023
Revised 14 June 2023
Accepted 18 June 2023
Available online 22 June 2023

ABSTRACT

The photoexcited triplet state of octaethylaluminum(III)-porphyrin (**AlOEP**) was investigated by time-resolved Electron Paramagnetic Resonance, Electron Nuclear Double Resonance and Electron Spin Echo Envelope Modulation in an organic glass at 10 and 80 K. This main group element porphyrin is unusual because the metal has a small ionic radius and is six-coordinate with axial covalent and coordination bonds. It is not known whether triplet state dynamics influence its magnetic resonance properties as has been observed for some transition metal porphyrins. Together with density functional theory modelling, the magnetic resonance data of **AlOEP** allow the temperature dependence of the zero-field splitting (ZFS) parameters, D and E, and the proton $A_{ZZ}$ hyperfine coupling (hfc) tensor components of the methine protons, in the zero-field splitting frame to be determined. The results provide evidence that the ZFS, hfc and spin–lattice relaxation are indeed influenced by the presence of a dynamic process that is discussed in terms of Jahn-Teller dynamic effects. Thus, these effects should be taken into account when interpreting EPR data from larger complexes containing **AlOEP**.


## 1. Introduction

Porphyrin derivatives are among the most versatile molecules in nature. Examples are the chlorophylls, employed in photosynthesis for solar energy conversion, and the hemes, used in respiration for oxygen transport and as electron carriers in oxidation and reduction catalytic reactions. In addition to their biological significance, porphyrin derivatives are also used extensively for a variety of applications such as artificial photosynthesis [1–3], dye-sensitized solar cells [4,5], molecular electronics and photonics [6,7], molecular catalysis [8,9] and photodynamic therapy [10]. The versatility of the porphyrins arises from the extended π-conjugation of the tetrapyrrole ring, its ability to bind a wide variety of substituents on its periphery and various elements in its center. The π-conjugation makes the porphyrins ideal for photochemical applications because it results in strong absorption of visible light and comparatively long excited singlet state lifetimes. Substituents on the periphery can be used to shift the absorption wavelengths and control the solubility properties. The element bound at the center of the tetrapyrrole ring can act as a catalytic site and influences the oxidation and reduction potentials of the conjugated π-system. Insertion of an Al(III) ion, for example, gives the porphyrin properties that make it a good redox active photosensitizer in supramolecular systems for artificial photosynthesis [1]. Such complexes can be constructed by attaching electron donors, acceptors and/or chromophores on opposite faces of the porphyrin ring via a covalent ester or ether linkage on one face and a Lewis acid-base coordination bond on the opposite face. The axial covalent bonding can also be used to form co-facial porphyrin dimers that mimic the special pair chlorophyll dimers found in natural photosynthesis [11].

Recently, we studied the excited state properties of one such dimer in which Al(III) octaethylporphyrin (**AlOEP**, Fig. 1) was

* Corresponding authors.
*E-mail addresses:* antonio.barbon@unipd.it (A. Barbon), marilena.divalentin@unipd.it (M. Di Valentin).
[1] Angelo Carella and Susanna Ciuti have contributed equally.

https://doi.org/10.1016/j.jmr.2023.107515
1090-7807/

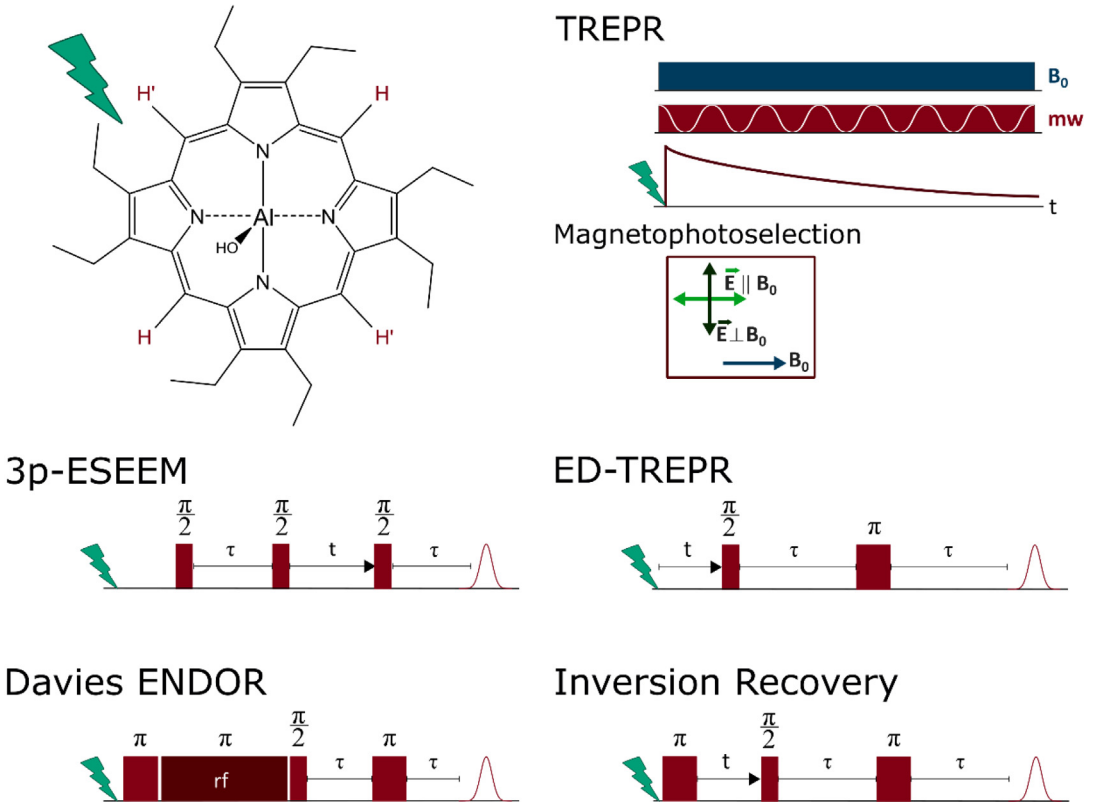


**Fig. 1.** Top left: chemical structure of **AlOEP**, where the two sets of equivalent methine protons are indicated. Top right: schematic representation of the Time-Resolved EPR (TREPR) experiment, including the use of linearly polarized light for magnetophotoselection. Bottom: pulse sequences of the experiments performed in this work: 3-pulse Electron Spin Echo Envelope Modulation (3p-ESEEM), Davies Electron Nuclear DOuble Resonance (ENDOR), Echo-Detected Time Resolved EPR (ED-TREPR) and Inversion Recovery.

linked to a phosphorus porphyrin [12]. The Time-Resolved Electron Paramagneti Resonance (TREPR) spectra of this complex showed interesting solvent dependent changes in the zero-field splitting (ZFS), which we ascribed to changes in the charge-transfer character of its delocalized triplet state. For such investigations, information on the behaviour of the triplet state of the corresponding porphyrin monomers can be invaluable to help distinguish between local dynamic effects within the monomers versus delocalization effects in larger multi-porphyrin complexes. The EPR characterization can be particularly useful in understanding the behaviour of the triplet state, but the data on main group porphyrins such as **AlOEP** is sparse. Thus, we have undertaken a detailed study of the magnetic properties of **AlOEP** using several time-resolved and pulsed electron paramagnetic resonance (EPR) methods.

TREPR, Electron-Spin Echo (ESE) techniques and pulsed Electron Nuclear DOuble Resonance (ENDOR), when coupled with photoexcitation, are ideally suited for investigating the electronic structure and dynamics of chromophores in their triplet state [13–17].

From the spin-polarized triplet state TREPR spectra it is possible to extract information about the zero-field splitting (ZFS) tensor and the triplet-sublevel dependence of the intersystem crossing rates. The ZFS parameters $D$ and $E$ are sensitive indicators of the spatial extension and symmetry of the excited triplet state, and the spin polarization properties are a fingerprint for the mechanism of its formation [15]. The time-evolution of the TREPR spectrum and specific ESE pulse sequences, *i.e.*, inversion recovery and echo-detected TREPR (ED-TREPR), can also be used to obtain information on spin dynamics and kinetic properties of the triplet spin sublevels [18,19].

Photoselective TREPR is an excellent method for quantitative determination of the relative orientation of the triplet-state ZFS axes and the optical absorption transition dipole moments [20–22]. It also allows these axes to be fixed in the molecule if the orientation of one of them is known or can be determined *in silico*.

Additional and more specific information about the unpaired electron spin distribution is obtained from the interaction of the triplet state with magnetic nuclei of the molecule, *i.e.* the electron-nuclear hyperfine couplings (hfcs). The isotropic hfc ($a_{iso}$) reflects the unpaired electron spin density at the respective nucleus and the anisotropy of the hyperfine tensor (**T**) is determined by the dipolar coupling between the electron and nuclear magnetic moments and hence it depends on the molecular geometry in the vicinity of the nucleus. However, the splitting of the EPR transitions due to the hfcs is not usually resolved in triplet-state EPR powder spectra. Thus, to determine the hfcs more advanced methods like ENDOR and Electron Spin Echo Envelope Modulation (ESEEM) experiments are required [23–27]. If the hfcs of several nuclei in different parts of the cofactor(s) can be determined and assigned to specific nuclei, the spin density distribution of the triplet state in the molecule is revealed. Pulse ENDOR and ESEEM combined with pulsed laser excitation at low temperatures are well suited for this purpose, since these hyperfine spectroscopies can take full advantage of the large electron spin polarization of the chromophore in the triplet state [28,29] compared to continuous light excitation and continuos wave-ENDOR methods.

The core of a metalloporphyrin is a tetrapyrrole ring with $D_{4h}$ symmetry. Its lowest excited triplet state is doubly degenerate with $^3E_u$ symmetry [30,31] and hence, its ZFS tensor is axially symmetric and the four methine protons at the meso positions are

magnetically equivalent (see Fig. 1). However, static distortions and vibronic coupling can break the symmetry and lift the degeneracy of the triplet states. This results in a loss of the axial symmetry of the ZFS tensor and inequivalence of these protons. If the energy difference between the two lowest triplet states is small enough to allow thermally induced transitions between them, averaging of the magnetic interactions in the two states occurs. If the rate of the transitions is higher than the frequency difference between interactions in the two states, the ZFS becomes axially symmetric and the hyperfine coupling to the four methine protons is the same. If transition rate is slower than the frequency difference, the ZFS tensor remains rhombic, and the four protons are not equivalent. This effect is known as the dynamic Jahn-Teller effect [32–35] and leads to changes in the rhombicity of the ZFS tensor and the hyperfine couplings as a function of temperature. The size of this effect depends on subtle details of the porphyrin structure and is difficult to predict *a priori*.

Here, we employ a range of light-induced EPR techniques to investigate in detail the triplet state of **AlOEP**. We show that the ZFS tensor obtained from the TREPR spectra becomes increasingly axial with increasing temperature as has been observed previously for Mg and Zn porphyrins [36,37], and has been interpreted as due to a dynamic Jahn-Teller effect. ENDOR and ESEEM measurements reveal that the hyperfine couplings to the methine protons are also strongly temperature dependent as expected from the proposed dynamic Jahn-Teller effect. However, in contrast to the Mg and Zn porphyrins, the presence of axial ligands in AlOEP plays an important role in the orientation dependence of the spin–lattice relaxation and temperature dependence of the hyperfine couplings.

## 2. Results

### *2.1. TREPR and pulse EPR: ZFS parameters, spin polarization and spin–lattice relaxation*

In this section we present X-band TREPR results for the triplet state of **AlOEP** in a glass-forming solvent at T = 10 K and 80 K. From the spin polarization patterns and magnetophotoselection data, the ZFS parameters and the orientation of the principal axes of the ZFS tensor with respect to the optical transition dipole moments have been obtained at the two temperatures. The spectral dependence of the spin polarization decay gives insight into the orientation dependence of the spin–lattice relaxation.

Fig. 2 shows a comparison between the X-band TREPR spectra of **AlOEP** in the glass phase of a 3:1 mixture of 2-methyltetrahydrofuran: dichloromethane (MeTHF:DCM) at 10 and 80 K. The spectra are extracted from the 2D data sets in a time window around the maximum of the EPR signal and are the weighted sum $(I_{\parallel} + 2I_{\perp})$ of spectra taken with the polarization of the excitation beam parallel $(I_{\parallel})$ and perpendicular $(I_{\perp})$ to the magnetic field to remove any photoselection effects. Simulations of the triplet spectra are shown in Fig. 2 (dashed spectra) and the parameters obtained from them are presented in Table 1. The simulations do not yield the signs of $D$ and $E$ directly but only the absolute value and therefore we report only the absolute values. However, both parameters been taken as positive based on self-consistent field theory (CASSCF) calculations and on the ENDOR data that will be discussed below. With this sign choice, the relative population rates $p_x$ and $p_y$ are equal and larger than $p_z$, as previously reported

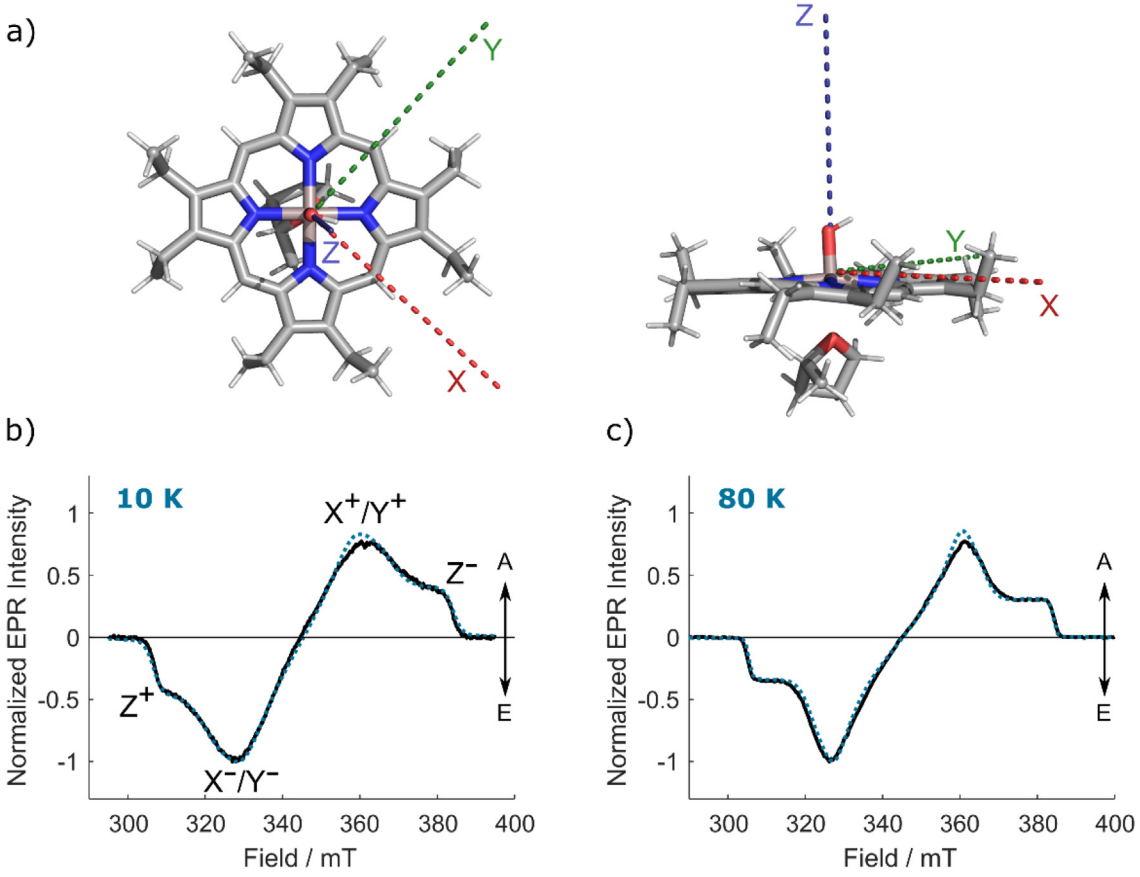


**Fig. 2.** (a) Top and side view of the orientation of the ZFS tensor principal axes (x = red, Y = green, Z = blue) in the **AlOEP** molecular frame, including a solvent molecule (MeTHF), obtained from Density Functional Theory (DFT) calculations. Experimental (black, solid) and simulated (blue, dashed) triplet state TREPR spectrum of **AlOEP** in a glassy 3:1 mixture of MeTHF:DCM, recorded at 80 K. (b) and at 10 K (c). Simulation parameters are reported in Table 1.

**Table 1**
ZFS parameters $D$ (±8 MHz) and $E$ (±5 MHz), relative triplet sublevel populations* (±0.05), and spin–lattice relaxation time constant (±1 μs at 10 K and ±0.2 μs at 80 K) derived from simulation of the TREPR spectra at 80 K and 10 K. For the decay constants, see text.

| | $p_x$:$p_y$:$p_z$ | $\|D\|$ (MHz) | $\|E\|$ (MHz) | $T_{1x}$ (μs) | $T_{1y}$ (μs) | $T_{1z}$ (μs) |
|---|---|---|---|---|---|---|
| 10 K | 0.43: 0.42: 0.15 | 1092 | 100 | 17 | 17 | 14 |
| 80 K | 0.42: 0.39: 0.19 | 1105 | 61 | 0.8 | 0.8 | 0.6 |

*The population ratios correspond to $D$, $E > 0$ as predicted by CASSSCF-NEVPT computations [12] and confirmed by the ENDOR data presented below.

[12]. It is apparent from the spectra in Fig. 2 and the parameters in Table 1 that the relative population rates, and hence the polarization patterns, are essentially the same at 10 and 80 K. Similarly, the total width of the spectrum, which is determined by the ZFS parameter $D$, is not strongly affected by the temperature and is only ∼1% larger at 80 K. In contrast, the value of $E$ obtained from the simulations is reduced by ∼40% at 80 K compared to 10 K, although the ZFS tensor remains orthorhombic. In the literature a decrease in $|E|$ with increasing temperature, observed in related porphyrins, has been ascribed to dynamic Jahn-Teller averaging [33]. We note that for the $X^+/Y^+$ transitions the experimental signal is always slightly less intense than the simulation for all recorded spectra while the $X^-/Y^-$ intensity is reproduced. This indicates that absorptive $X^+/Y^+$ transitions are weaker than the emissive $X^-/Y^-$ for these orientations and hence, the spin system displays weak net emissive polarization. We have shown previously that such net polarization can be generated by back-and-forth transitions between two triplet states with ZFS axes related to one another by a rotation about the z-axis [38,39]. Such a situation can occur in porphyrins if the degeneracy of the lowest triplet state is lifted slightly due to the Jahn-Teller effect and thermally activated transitions between the two states can take place.

To further characterize the triplet state ZFS tensor, we carried out magnetophotoselection experiments. Fig. 3 shows the TREPR spectra of **AlOEP** in the glass phase of a 3:1 mixture of MeTHF: DCM at 80 K with the plane of the laser polarization parallel (red spectrum) and perpendicular (blue spectrum) to the magnetic field. The transitions at 544 nm (Fig. 3b) and at 576 nm (Fig. 3c), corresponding to the two $Q$-bands of the electronic absorption spectrum, were used for excitation. Since the experimental setup assured the same excitation conditions for the two polarization orientations, the spectra are displayed without renormalization and show an evident magnetophotoselection effect, with enhanced $X$ and $Y$ triplet transitions with the parallel orientation and enhanced $Z$ transitions with the perpendicular orientation. Neither the magnetophotoselection effect nor the ZFS parameters show any significant wavelength dependence. Simulations of the spectra were carried out using the parameters given in Table 1 and include the relative orientation of the ZFS axis system and the electric transition dipole moments as variable parameters. The simulations show that the transition dipole moment(s) and the $X$ and $Y$ principal axes of the ZFS tensor lie in the same plane. Complete active space CASSCF calculations predict that the $Q_x$ and $Q_y$ optical transitions are degenerate [12], suggesting that the two $Q$-bands observed in the spectrum are part of a vibrational progression [40]. This means that the $Q_x$ and $Q_y$ transitions cannot be excited separately, and hence it is only possible to determine that the $X$ and $Y$ principal axes of the ZFS tensor lie in the same plane as the $Q_x$ and $Q_y$ transitions but not their orientations within the $xy$ plane. The calculations also predict that the two transition dipole moments are orthogonal to one another and lie in the porphyrin plane as do the $X$ and $Y$ axes of the calculated ZFS tensor, in agreement with the magnetophotoselection result.

Triplet state kinetics, including dynamic and relaxation processes, can be investigated by analysis of the time evolution of the spin polarization. The time dependence of the TREPR signals represents the motion of the magnetization in the rotating frame and depends on spin-relaxation, precession of the magnetization about the effective field and decay of the excited triplet state. In the limit of low microwave power and for a long-lived triplet state with $T_1 \gg T_2$, the decay of the polarization determined by the TREPR experiments is dominated by $T_1$ [41]. Alternatively, ED-TREPR and inversion recovery pulse experiments can be carried out to estimate the spin–lattice relaxation time.

Before collecting a full time/field dataset for kinetic analysis, we measured several transients at field positions corresponding to the ZFS canonical orientations to check for possible distortion due to response time limitations of the cavity. When these transients were fit as a sum of simple exponentials, the lifetime of one of the components was close to the response time of the critically-coupled cavity. Therefore, we decided to reduce the response time of the cavity by over-coupling it to reduce its Q-factor. To determine what Q-factor gave an undistorted signal, we used the ED-TREPR signal as a reference. The ED-TREPR method (Fig. 1) is

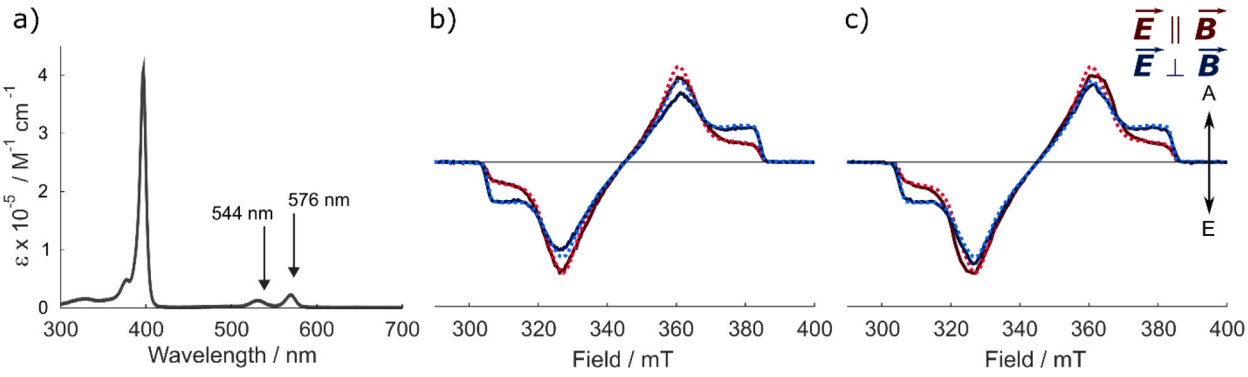


**Fig. 3.** Magnetophotoselection and wavelength dependence of the triplet state TREPR spectra of **AlOEP.** (a) UV/VIS absorption spectrum for **AlOEP** in DCM at room temperature. (b) Experimental (solid) and simulation (dashed) triplet state TREPR spectrum of **AlOEP** in a glassy 3:1 mixture of MeTHF:DCM, recorded at 80 K, after photoexcitation at 544 nm with light linearly polarized parallel (red) and perpendicular (blue) to the magnetic field. (c) Corresponding TREPR spectra of **AlOEP** after photoexcitation at 576 nm. All other parameters are the same as for panel b). Simulation parameters are reported in Table 1.

characterized by excellent time resolution at the cost of lower signal intensity and long acquisition time. At several field points corresponding to the principal orientations ZFS tensor we confirmed that the TREPR transients collected with the cavity over-coupled were undistorted with respect to the corresponding ED-TREPR transients (see Figs. S1 and S2). We then collected a full time/field dataset for analysis.

The dataset and its simulation are summarized in Fig. 4. In Fig. 4a, the calculated full time/field TREPR dataset is compared with the experimental dataset at 80 K. Fig. 4b shows the triplet

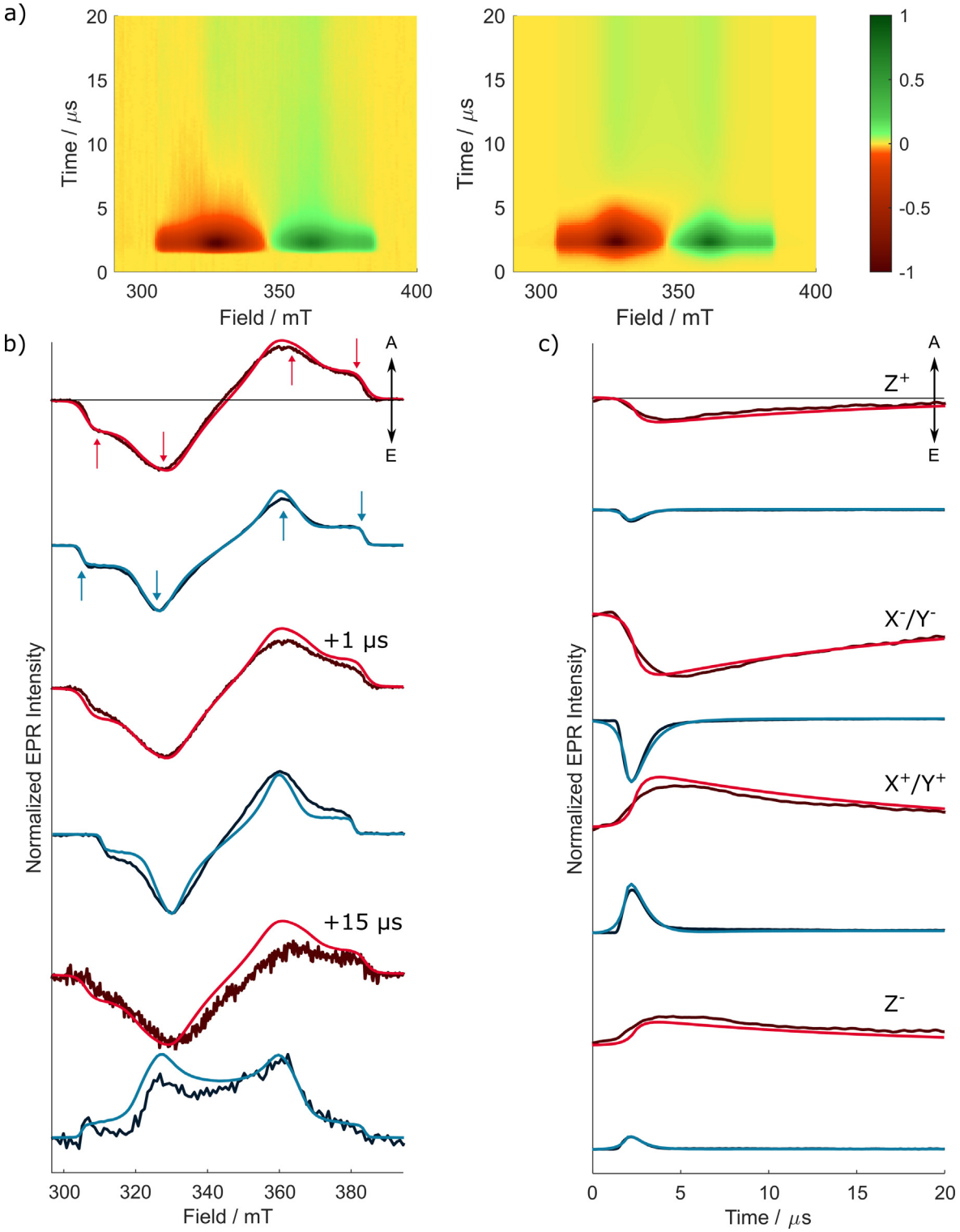


**Fig. 4.** (a) Experimental (left) and simulated (right) contour plots of the 2D TREPR data for the triplet state of **AlOEP** in a glassy 3:1 mixture of MeTHF:DCM, recorded at 80 K. The corresponding 2D TREPR data at 10 K is reported in Fig. S1. (b) Variation of the TREPR spectra at 10 K (dark red) and 80 K (dark blue) at different delays from the maximum of the signal (0, 1, 15 μs) and corresponding simulation (light red and blue, respectively). (c) Time evolution of the TREPR signal at 10 K and 80 K measured with an over-coupled resonator, recorded at the canonical ZFS turning points (indicated by the arrows) and the corresponding simulations, colour code as in (b). Simulation parameters are reported in Table 1.

powder spectra at selected time delays after flash (DAF) with the corresponding simulations. Time traces at selected field positions indicated by the red arrows in Fig. 4b are shown in Fig. 4c. To better facilitate comparison of the evolution of the dataset at 10 K and 80 K, data at the two temperatures are shown together in Fig. 4b and c. The simulations at 80 K are shown in dark blue and those at 10 K are in red. As can be seen in Fig. 4b, at 80 K (dark blue), the early detected spectrum with polarization *eee/aaa* (*e*: emissive, *a*: absorptive) for the three feature pairs evolves to a purely absorptive spectrum at 15 μs, with a lineshape close to that expected for a Boltzmann population distribution. In contrast, at 10 K, the shape of the spectrum remains almost unchanged also after 15 μs.

The simulation of the time evolution of the intensity was obtained considering the time variation of the population by solving the master equation [42,43], in which both the spin–lattice relaxation time $T_1$, and the decay to the ground state were considered as described in the Materials and Methods section (Eq. (2)). In this treatment the time dependence of the signal is assumed to arise only from the time dependence of the populations of the stationary states of the Hamiltonian. The microwave field is not explicitly included, and precession of the magnetization is ignored. Such a treatment is valid for slowly decaying signals measured with low microwave power. In this case, the off-resonant and coherent contributions that decay within a few tens of ns are not resolved and only exponential decay of the signal by $T_1$ relaxation and/or decay to the ground state is observed. To ensure that these conditions were met, we compared $T_1$ values obtained by model fitting with the values obtained from the ED-TREPR and ESE inversion-recovery experiments at the canonical transitions (see Fig. S2) and found that they are in good agreement. The kinetic parameters derived from the simulations of full time/field TREPR dataset are reported in Table 1. The slowest component of the signal decay is found to be on the order of a few hundreds of μs, as evaluated for example from the ED-TREPR traces and is similar to the room temperature lifetime of the **AlOEP** triplet state (86 μs) [11]. The faster components observed in the time window of the TREPR experiments (20 μs) can therefore be ascribed to $T_1$ relaxation and can be used to discuss dynamical effects on the molecule.

The strong temperature dependence of the $T_1$ relaxation is expected since modulation of the highly anisotropic ZFS by either molecular and/or electronic motion provides an effective $T_1$ relaxation mechanism that can account for the experimental observations. It has been shown that if a second low-lying triplet state is thermally accessible and has ZFS axes that are rotated with respect to the lowest excited triplet state, temperature dependent spin–lattice relaxation caused by the modulation of the ZFS is observed [44]. Since we observe temperature dependent changes in the ZFS parameters (Table 1) and the lowest triplet state of **AlOEP** is (nearly) degenerate, the change in the relaxation rate is likely due to modulation of the ZFS as would be expected from the dynamic Jahn-Teller effect.

### 2.2. ENDOR and ESEEM: Hyperfine structure

Experimental studies of the spin-polarized triplet state of **AlOEP** by TREPR are complemented by pulse ENDOR and ESEEM measurements to provide more detailed information about the unpaired electron spin distribution at specific positions of the macrocycle. The bridging methine protons at the four meso positions are characterized by large negative spin densities and can serve as sensitive probes.

The significant anisotropy of the triplet state ZFS tensor, in comparison to that of the hfcs, allows orientation-selective hyperfine spectroscopy to be performed and provides the orientation of the hfc tensor components ($A_{ii}$) relative to the ZFS tensor axes, which include the Fermi-contact $a_{iso}$ and the dipolar interaction component $T_{ii}$ ($A_{ii} = a_{iso} + T_{ii}$). Excitation is performed at the turning points of the triplet spectrum where the external field is mainly parallel to one of the ZFS canonical axes. In addition, in contrast to doublet states, the ENDOR spectra of triplet states allow direct determination of the signs of the hfcs (see Fig. 5) if the sign of the ZFS parameter D is known. Analogous considerations apply to ESEEM, as the periodic modulation of the local field experienced by the electron spin provides information about the hyperfine frequencies if the hyperfine principal axes deviate from the ZFS tensor axes.

Fig. 5a shows the splitting of the spin energy levels of the triplet state at high field ($B_0$) for the three canonical orientations X, Y, and Z. In the diagram, the ZFS D parameter has been chosen to be positive, as expected for π-π* triplet states of porphyrin derivatives [15] and confirmed by magnetophotoselection experiments and published CASSCF calculations for **AlOEP** [12]. In Fig. 5b the spin energy levels are shown for the hyperfine interaction of the triplet spin (S = 1) with one proton spin (I = ½) in the high-field limit. As an example, we consider the triplet spin energy levels for the Z canonical orientation, which include the first-order hyperfine interaction $A_{ZZ}$ in the ZFS frame. A small interaction is assumed ($A/2 < \nu_H$). In the ENDOR spectrum, a strong and narrow line is expected at the Larmor frequency, $\nu_H$, arising from the $M_S = 0$ manifold, and a further ENDOR transition occurs either at higher or lower frequency depending on the sign of the hyperfine interaction tensor element.

The two ENDOR resonance frequencies according to the triplet ENDOR resonance condition [13] are:

$$\nu_{ENDOR} = |\nu_H - M_s A_{ZZ}| \quad (1)$$

For the $Z^+$ transition of a triplet state with D > 0, the ENDOR lines from the $M_s = +1$ manifold occur on the low (if $A_{ZZ} > 0$) or high (if $A_{ZZ} < 0$) frequency side with respect to the Larmor frequency of the proton, $\nu_H$. The opposite situation is encountered for the $Z^-$ transition, where the lines correspond to the $M_s = -1$ manifold.

ENDOR experiments of porphyrin triplet states performed with the magnetic field positioned at $Z^+$ or $Z^-$ in the EPR spectrum are selective for molecules oriented with their molecular (π) plane perpendicular to $B_0$, leading to a strong orientational selection and single crystal-like ENDOR spectra [45]. For methine protons, which are located in the plane of the π-system (see Fig. 1), the hfc tensor component along the Z ZFS axis ($A_{ZZ}$) corresponds to a very good approximation to the corresponding principal component of the hfc tensor [46], see Fig. S4.

The Q-band $^1$H Davies ENDOR spectrum of the triplet state of **AlOEP** in the glass phase of a 3:1 mixture of MeTHF:DCM, recorded at the $Z^-$ canonical field position (T = 10 K), is shown in Fig. 6a. In the corresponding inset, the echo-detected spectrum is reported to highlight the working field position. The ENDOR spectrum is plotted versus $\nu-\nu_H$ so that the proton Larmor frequency peak appears at zero. The ENDOR peaks corresponding to negative hyperfine components, as expected for the $A_{ZZ}$ components of the methine protons as they are α-protons, occur at lower frequencies with respect to the Larmor frequency for this specific EPR transition. Indeed, two broad ENDOR lines, which can be assigned to two distinct sets of methine protons based on the sign of the hfc, are present in the low-frequency region of the spectrum, as highlighted in the deconvolution of the spectrum. The corresponding hfcs are reported in Table 2.

The assignment is further corroborated by DFT calculations using the PBE-D3 functional and the def2-TZVP basis set. The orientation of the ZFS principal axes in the molecular frame from previously published CASSCF calculations [12] was used with the hyperfine tensor from the DFT calculations to obtain the values $A_{ZZ}$ given in Table 2. The calculations were repeated for several

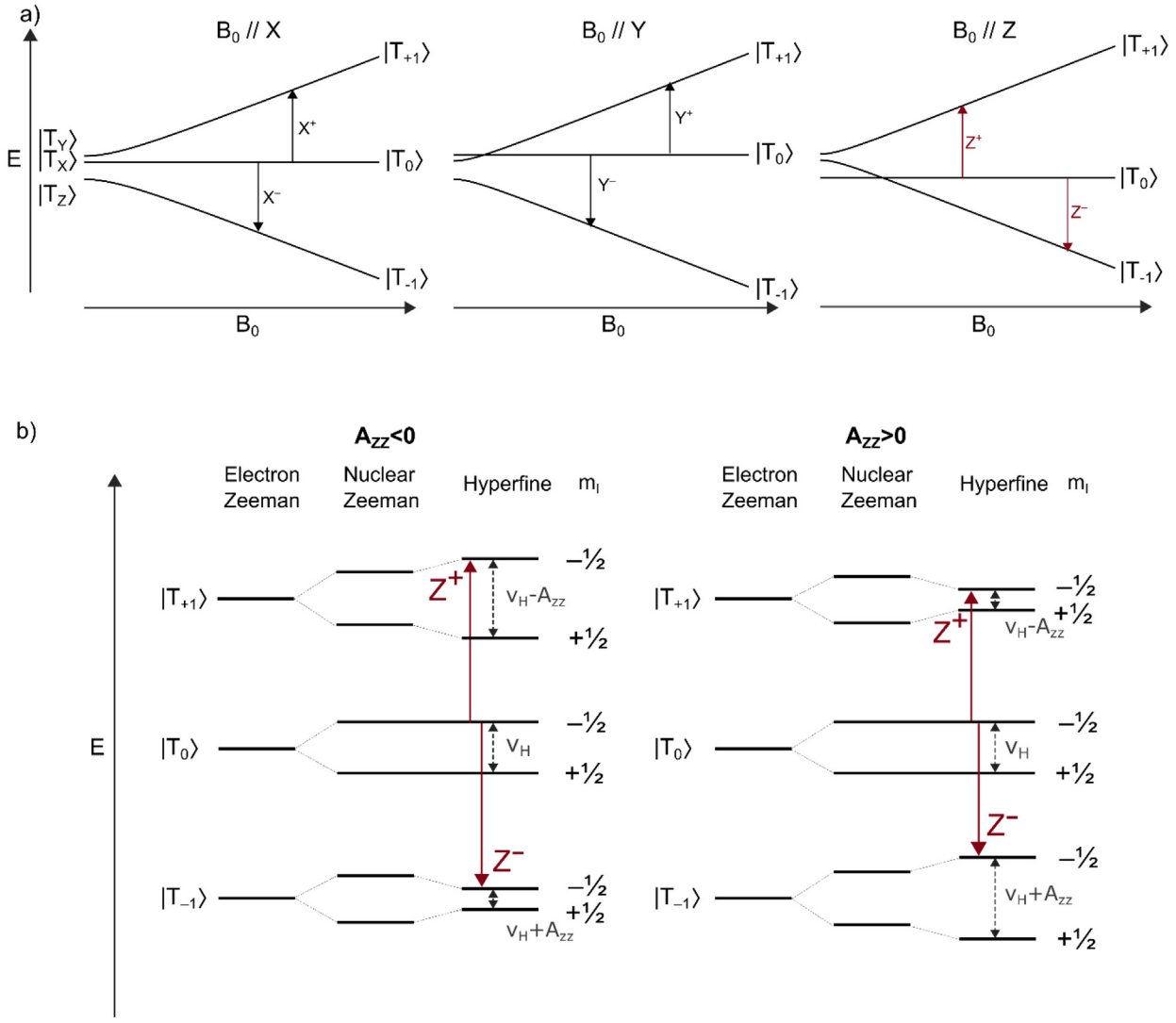


**Fig. 5.** (a) Energy diagram of the triplet spin sublevels as a function of the magnetic field $b_0$, for D > 0 and E > 0, with the field vector parallel to each of the principal axes of the ZFS tensor. The arrows indicate the two allowed canonical EPR transitions according to the selection rule $\Delta M_S = \pm 1$. (b) Energy scheme of a triplet state coupled to a single proton $^1H$ (I = ½) for $B_0$ parallel to the Z ZFS axis and positive and a negative hyperfine coupling constant $A_{ZZ}$. The red arrows indicate the EPR transition for $m_I = -½$; those for $m_I = +½$ are omitted. The dark grey arrows (dashed) indicate the ENDOR transitions. Note that the electron spin and ZFS energies are not to scale.

different conformers of the ethyl substituents but no significant effects were observed for the hfcs of the methine or ethyl protons (see Table S1). The corresponding ENDOR lines of the latter appear as a weak shoulder on the free proton line. The calculated values of $A_{ZZ}$, reported in Table 2, refer to two distinct cases: a six-coordinate geometry of Al(III), involving both the covalently bound hydroxyl group and a coordinated solvent molecule (MeTHF) or five-coordinate geometry involving only the hydroxyl group. The optimized structures in the triplet state with and without solvent coordination are shown in Fig. S4 in the Supporting Information. Calculations confirm the inequivalence of the methine protons and show that their hfcs strongly depend on the solvent coordination of Al(III). Better agreement between the calculated and experimental hfcs at 10 K is obtained when a coordinated solvent molecule is included in the DFT calculation.

In the ENDOR experiments measured with the field set to the positions of the X and Y canonical transitions, a variety of orientations with respect to the magnetic field are excited, which broadens the lines and complicates the corresponding spectrum. In Fig. S5 of the Supporting Information, the Q-band $^1H$ Davies ENDOR spectra, recorded for **AlOEP** in the triplet state at the $Y^+$ canonical field position, are reported and the broad $A_{YY}$ contributions of the methine protons are simulated, showing a satisfactory agreement with DFT calculations.

ENDOR experiments at higher temperatures were precluded by short relaxation times, therefore X-band 3p-ESEEM experiments were performed at 80 K in the glass phase of a of a 3:1 mixture of MeTHF:DCM to investigate the temperature dependence of the hfcs. The 3p-ESEEM frequency spectrum and the simulation at the $Z^+$ canonical field position are shown in Fig. 6b. In the corresponding inset, the echo-detected spectrum is reported in order to highlight the working field position. The ESEEM spectrum is plotted versus $\nu - \nu_H$ so that the proton Larmor frequency peak appears at zero. In addition to this peak, the spectrum in Fig. 6b shows proton hyperfine peaks around 5 MHz and strong $^{14}N$ peaks around −10 MHz. The $^{14}N$ region is dominated by the double-quantum frequency of the $M_s = 0$ manifold, as shown previously for Zn porphyrins [47,48]. As in the ENDOR experiments, the position of the proton hyperfine peaks relative to the free proton line depends on the sign of the hyperfine coupling and the value of

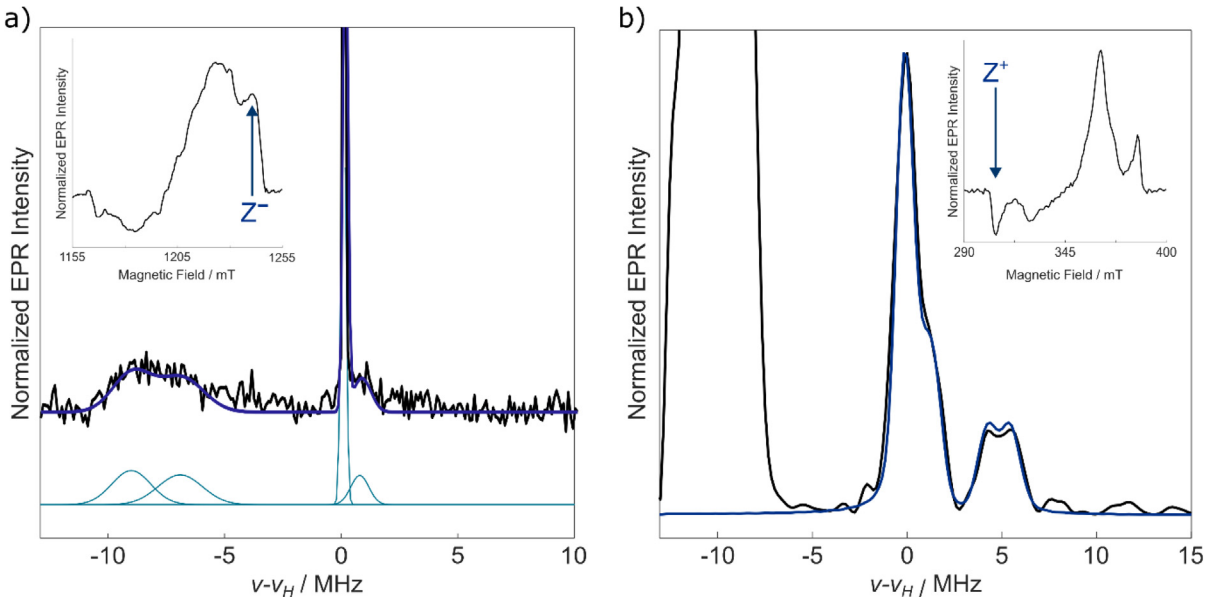


**Fig. 6.** (a) Triplet state Davies ENDOR spectrum of **AlOEP** in a glassy 3:1 mixture of MeTHF:DCM (black), recorded at 10 K and at Q-band; the overall best fit (blue) and the relative Gaussian deconvolution (light blue) are also shown. The resonance field corresponds to the $Z^-$ ZFS canonical transition, as indicated by the arrow in the field-swept ESE spectrum shown in the inset. (b) Triplet state 3p-ESEEM frequency spectrum of **AlOEP** in a glassy 3:1 mixture of MeTHF:DCM (black), recorded at 80 K and at X-band; the simulation is shown in blue. The resonance field corresponds to the $Z^+$ ZFS canonical transition as indicated by the arrow in the field-swept ESE spectrum shown in the inset. The hyperfine parameters are reported in Table 2.

**Table 2**
$A_{ZZ}$ in MHz for the methine protons of **AlOEP** in the triplet state, obtained from ENDOR experiments at 10 K (±0.5 MHz), 3p-ESEEM experiments at 80 K (±0.2 MHz) and DFT calculations.

| $A_{ZZ}$(MHz) | Solvent | Methine | Methine* |
|---|---|---|---|
| ENDOR | MeTHF/DCM 3:1 | −9.2 | −6.7 |
| 3p-ESEEM | MeTHF/DCM 3:1 | −5.9 | −4.3 |
| DFT | MeTHF | −8.54 | −6.91 |
| | No solvent | −5.70 | −5.15 |

* The methine protons are indicated in Fig. 1.

$M_S$. For the ESEEM experiment shown in Fig. 6b, the low field canonical transition was selected since the $^{14}N$ and the negative $^1H$ hfcs will appear on opposite sides of the proton Larmor frequency line and can, therefore, be easily distinguished. The peaks near 5 MHz can be assigned to the methine protons, since they are the only ones with significant negative $^1H$ hfcs in **AlOEP**. As can be seen in Fig. 6b, the peak near 5 MHz is broad and shows some structure suggesting that the methine protons are probably not equivalent. In the fitted spectrum, it has been modelled as two sets of protons, but the two peaks are not clearly resolved in the spectrum. As can be seen in Table 2, the methine proton hfc's obtained from the 80 K ESEEM experiment are significantly smaller than those at 10 K. Comparison with the hfcs from DFT calculations suggests that this may be the result of weaker coordination of the solvent at 80 K.

## 3. Discussion and conclusions

To a first approximation, the electronic structure of metalloporphyrins such as **AlOEP** can be modelled as a porphine ring with $D_{4h}$ symmetry (Fig. 7). Using this model, the lowest triplet state of porphyrins with substituents in the $\beta$-pyrrolic positions is described as an $a_{1u}$ $(\pi) \rightarrow e_g(\pi^*)$ excitation and is doubly degenerate with $^3E_u$ symmetry [30,31]. However, this degeneracy may be lifted by Jahn-Teller distortion of the plane of the molecule and/or asymmetry of the environment. As shown in Fig. 7, an in-plane distortion, which changes the ring symmetry from $D_{4h}$ to $D_{2h}$, lifts the degeneracy of the $^3E_u$ state generating $^3B_{2u}$ and $^3B_{3u}$ states. The values of E are equal and opposite in these two states, while D is the same. Depending on the temperature and the energy difference and barrier between these two states, back-and-forth transitions between them can occur resulting in a dynamic Jahn-Teller effect. If the transition rate is fast enough the ZFS tensor is averaged, and it becomes axial.

In the case of **AlOEP**, the axial ligands break the $D_{4h}$ symmetry and the lowest triplet state is not truly degenerate. Thus, it is perhaps more correct to refer to the distortions as a *pseudo* Jahn-Teller effect, but we will not use this term in keeping with the majority of the literature. While the idealized model shown in Fig. 7 should describe the general behaviour of the **AlOEP** triplet state, some deviations can be expected. For example, it is possible that in the two low-lying triplet states the values of E might not be exactly equal and opposite. Jahn-Teller distortions involving the axial ligands are also possible. These have been reported to influence the spin relaxation properties of six-coordinate Fe(III) porphyrins [49] and could also potentially play a similar role in **AlOEP**. They could also lead to differences in the values of D and the directions of the ZFS Z-axes in the two low-lying triplet states.

The analysis of the isotropically excited TREPR spectra, extracted from the 2D dataset at short delay after the laser pulse when the electron spin polarization is largest, shows that the ZFS tensor is orthorhombic ($E \neq 0$) in the temperature range under investigation (10–80 K), but there is a decrease in the rhombicity of the ZFS tensor at higher temperature ($\lambda=|E/D|$ are 0.092 ± 0.00 5 and 0.055 ± 0.005 at 10 K and 80 K, respectively), which suggests the presence of a dynamic Jahn-Teller effect. The triplet spin sublevel populations remain essentially constant over the temperature range. In the specific case of the in-plane populations ($p_x$ and $p_y$), their values are similar and therefore the amount of information on the Jahn-Teller effect that may be derived from a change of these parameters is limited. In Mg and Zn porphyrins, the Jahn-Teller averaging at temperatures around 80 K can be complete or only partial depending on the type of substituents and the coordinating properties of the solvent [36,37].

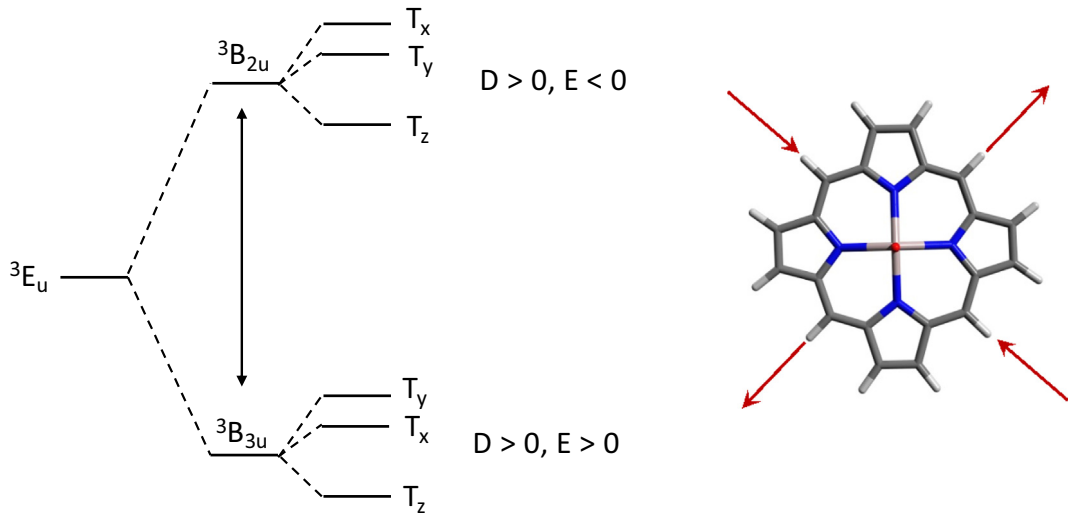


**Fig. 7.** Influence of a static Jahn-Teller distortion of an idealized porphine ring with $D_{4h}$ symmetry on the triplet state energy levels [31]. Distortion of the ring as indicated by the red arrows lifts the degeneracy of the $^3E_u$ state. The $^3B_{3u}$ state has been placed lowest in energy based on the positive value of E obtained from CASSCF calculations of **AlOEP**.

The dynamic Jahn-Teller effect can also make an important contribution to the spin–lattice $T_1$ relaxation [50,51]. As discussed above, the relaxation rate $1/T_1$ increases by nearly an order of magnitude at 80 K compared to 10 K (Table 1). A similar temperature dependence has also been reported for Zn(II) tetratraphenylporphyrin and other Zn analogues [36,37]. For Zn porphyrins, the Jahn-Teller distortion consists of alternate elongation of the molecule along each of the two perpendicular in-plane symmetry axes, resulting in a reduction the symmetry from $D_{4h}$ to $D_{2h}$ as shown in Fig. 7. The two forms are symmetry-related [35] and strong anisotropic relaxation is produced when they can exchange by a thermally activated interconversion that acts as a pseudorotation, in which the Z-axis of the ZFS tensor is preserved, but the X and Y principal directions are exchanged. The process of interconversion then provides a contribution to the spin–lattice relaxation, which is dependent on the interconversion rate and the value of E, that is a measure of the ZFS anisotropy in the XY plane [39]. As a consequence, the time-dependence of the triplet spectra is characterized by a strongly anisotropic temperature dependent relaxation behaviour with the X and Y ZFS components relaxing more rapidly than the Z transition at higher temperature.

In **AlOEP**, the spin–lattice relaxation does not show the strong orientation dependence observed in Zn porphyrins. As can be seen in kinetic parameters obtained from simulation of the time-evolution of the triplet spectrum (Table 1) the $T_1$ values are essentially the same for all three canonical orientations but are much shorter at 80 K than at 10 K. This reduction in $T_1$ is not accompanied by any substantial change in the ZFS parameter D. Since modulation of the ZFS is expected to be the main mechanism for $T_1$ relaxation and is known to be responsible for the relaxation of the X and Y components in Zn porphyrins, the data suggest that modulation of the Z component also occurs in **AlOEP** but that its average value is essentially unaffected. An obvious difference between the Zn porphyrins and **AlOEP** is the presence of axial ligands in the latter. An out-of-plane Jahn-Teller distortion has been implicated in the relaxation properties of axially coordinated Fe(III)-substituted porphyrins [49] and we speculate that this may also be responsible for the temperature dependent relaxation of the Z component in **AlOEP**. Unlike the in-plane motions that cause interconversion of the X and Y components and a reduction in E, out-of-plane motions involving the axial ligands could modulate D without changing its average value or the orientation of the z-axis.

Magnetic interactions other than the ZFS can also be affected by Jahn-Teller distortions. For example, in Cu(II) complexes, the dynamic Jahn-Teller effect has been observed as a vibronic averaging of the **g** and **A** tensors [52–54], but these effects have never been investigated in porphyrin systems. For this reason, we performed both pulse ENDOR and ESEEM experiments on **AlOEP** at 10 and 80 K, respectively. ENDOR was not feasible at 80 K since the electronic relaxation times are too short to use a radio frequency pulse with the appropriate length in the ENDOR sequences, while the relaxation conditions are still favourable for the 3p-ESEEM experiment. The fast detection scheme of ESEEM allows the mapping of proton ENDOR frequencies at higher temperatures. Usually, ESEEM is used to detect nuclei with a small gyromagnetic ratio, but proton ESEEM can be useful when a temperature dependence is investigated. Furthermore, single crystal-like ESEEM may be possible for photoexcited triplet states by recording ESEEM spectra at the magnetic fields relative to the Z features. The limitation of ESEEM is that traces need to be recorded outside of the hyperfine tensor canonical directions: if the ZFS and hyperfine frames are collinear a very weak, or null, modulation amplitude is expected if ESEEM is recorded at the Z-resonant field positions. This can, however, be overcome by moving the resonance field slightly to select resonant molecules having a tilt angle (*i.e.*, ~20°) with respect to the principal orientations of the hyperfine tensor [29].

Hyperfine spectroscopy on **AlOEP** allows detection of the hfcs of the methine protons, which are characterized by a large, negative isotropic contribution and a strongly anisotropic dipolar contribution, as shown by DFT calculations. The $A_{ZZ}$ component, in the ZFS frame, was detected both at 10 K and at the higher temperature by excitation near the Z triplet transition. ENDOR spectra obtained from excitation near the Y transitions show a severe broadening of the lines that can be ascribed to incomplete orientation selection and/or slow Jahn-Teller interconversion rate between slightly different triplet states.

Two different hfcs corresponding to two different sets of methine protons have been detected in both the 80 K ESEEM and 10 K ENDOR spectra. The inequivalence of the four methine proton is predicted by DFT calculations and has also been reported for the free-base porphine [55,56]. A single signal from the meso protons should only occur if the porphyrin ring has four-fold symmetry. The comparison of the ENDOR and ESEEM spectra shows that at

80 K the frequency difference between the two methine proton lines is reduced as is the average of the two frequencies. Since the hfcs at 80 K are close to the calculated values without a coordinated solvent molecule, we speculate that distortion of the molecule in the axial direction may occur and that a triplet state with weaker coordination of the solvent becomes accessible at higher temperature. This is also consistent with the strong reduction in the spin–lattice relaxation time at 80 K compared to 10 K.

There are very few reports of the averaging of hyperfine couplings in Jahn-Teller systems [52,54], and the data in the literature have been collected mostly at very low temperatures where the spin–lattice relaxation time is sufficiently long to be measured and where the Jahn-Teller dynamics are very slow. In addition, most of the ENDOR studies of porphyrins in the literature have been caried out on *meso*-substituted porphyrins [21,47,56,57] compared to the β-substituted porphyrin reported here. Elucidation of the electronic structure of β-substituted metalloporphyrins is particularly important since substituents are only found at these positions in naturally occurring porphyrins and chlorins. The data presented here confirm that bridging methine protons are characterized by a rather large negative spin density, as predicted by DFT calculations and in agreement with the large methine hfcs reported for free-base porphine [55].

The spin density distribution on the nuclei is closely related to the electronic wavefunction, since it probes the coefficients of the atomic orbitals contributing to the HOMO and LUMO where the two unpaired electrons are localized. Tuning of the hfcs and consequently of the spin density distribution is not easily achieved in porphyrins and an active role is probably played by the coordination chemistry of Al(III) which produces subtle distortion effects of the macrocycle. This finding complements the characterization of the dynamic behavior of Al porphyrins, showing that the coordination properties of Al(III) can produce strong effects in terms of the electronic structure and consequently on the reactivity and photochemical properties of the tetrapyrrole macrocycle.

In contrast to the large body of EPR and Optically Detected Magnetic Resonance investigations yielding D and E parameters, which are integral properties of the triplet wavefunction and depend on its overall spatial distribution, there are only a limited number of studies on the hyperfine structure of the triplet state of porphyrins resolved by hyperfine spectroscopy [21,47,56–60]. Similar to TREPR, pulsed ENDOR and ESEEM of photo-excited triplet states take advantage of their large spin polarization. The light-induced polarization of triplet spin label/probes has been shown to provide an important increase in sensitivity for dipolar spectroscopy and distance determination [61–63]. The same reasoning should apply to hyperfine spectroscopy which take full advantage of the large electron spin polarization of the triplet state compared to the corresponding application to radical cations and anions, while probing the electron distribution of both the HOMO and the LUMO in the same experiment.

In summary, the magnetic and dynamic parameters of **AlOEP** in the triplet state were determined using the complete gamut of light-induced advanced EPR techniques and complemented with theoretical methodologies, providing a reliable and detailed picture of the electronic structure and assessing the symmetry of a representative member of this important class of heterocyclic tetrapyrrolic compounds. The data indicate the involvement of a dynamic Jahn-Teller effect that leads to partial averaging of the magnetic parameters at higher temperature. The data also suggest that axial ligands can play an important role in the Jahn-Teller dynamics. The effect on the hyperfine interaction of the methine protons and on the anisotropy of the spin–lattice relaxation both point towards distortion of the axial coordination bond that modulates Z component of the ZFS and the spin density at the meso positions of the porphyrin ring. This detailed picture underlines that, in the presence of Al(III) coordination, the porphyrin triplet state is characterized by unique properties when compared to other metalloporphyrins, which are commonly employed in diverse applications including artificial photosynthesis.

## 4. Materials and methods

### 4.1. Sample preparation

The synthesis of the porphyrin has been described previously [11]. Samples were prepared dissolving the porphyrin in the solvents of choice. Samples were prepared in a 3:1 mixture of MeTHF: DCM with a concentration of about 500 μM. TR-EPR and pulse experiments (ESEEM, ED-TREPR, Inversion Recovery) were additionally performed on a sample prepared in a 9:1 mixture of MeOH: glycerol at the same concentration. X-band samples were prepared inserting the solution inside 4 mm o.d. quartz tubes which were sealed under vacuum after few freeze–pump–thaw cycles. Q-band samples were prepared in a glovebox, inserting the solution inside 1.6 mm o.d. quartz tubes which were sealed under vacuum after a few freeze–pump–thaw cycles.

### 4.2. EPR measurements

EPR measurements at 80 K were performed on a Bruker Elexsys E580 spectrometer and operating at X-band and equipped with a dielectric MD5 resonator. Photoexcitation was obtained using a Quantel Rainbow Nd:YAG pulsed laser equipped with second and third harmonic modules and with an optical paramagnetic oscillator (OPOTECH) for irradiation at variable wavelength within the visible, working at 10 Hz, with pulse length of 5 ns and an energy of 3–5 mJ/pulse. Temperature stability was assured by an Oxford CF935 dynamic continuous-flow cryostat cooled with liquid nitrogen and controlled by Oxford ITC503 units.

TREPR spectra were obtained by accumulating typically 100–120 traces of the unmodulated EPR signal coming out from the diode detector after a 6 MHz bandwidth preamplification stage. The digitalization of the traces was performed by externally connected LeCroy digital oscilloscopes (series 9300). The cavity was maintained either in critically coupled condition or with a Q-value lower by a factor of 0.5 ca. to have a faster time response. Field-independent time traces contributions, deriving from the cavity and obtained as averaged off-resonance high field and low field traces, were subtracted.

The microwave power was near 0.2 mW. Magnetophotoselection experiments were performed by irradiating the sample with polarized laser pulses, with the electric field either parallel or perpendicular to the static magnetic field. The rotation of the polarization plane of the light was obtained with a half waveplate and a linear polarizer was added for a better control of the polarization.

Evolution of the magnetization with time was also recorded by pulse methods, measuring the 2-pulse echo intensity for variable delays between the laser flash and the first pulse (ED-TREPR). The delay between the pulses was set to 300 ns and a π/2 pulse of 16 ns was used. The inversion recovery experiment was performed by applying the sequence laser-DAF-(π)-$t_1$-(π/2)-$t_2$-(π)-$t_2$, increasing the time $t_1$ starting from a value of 300 ns with increments of 100 ns. The DAF was 56 ns; a π/2 pulse of 16 ns was used.

3p-ESEEM experiments were performed by applying the echo sequence laser-DAF-(π/2)-$t_1$-(π/2)-$t_2$-(π/2)-$t_1$. The DAF was 200 ns, delay $t_1$ was set to 180 ns, while the initial $t_2$ to 300 ns. After removal of the decaying component, the spectrum was then obtained by application of a Hamming function followed by zero-filling to 1024 points and Fourier transform of the signal. In order to cope with the variation of the modulation depth as a function of

the molecular orientation, which alters the ESEEM lineshape, the 3p-ESEEM spectrum was simulated with EasySpin [64] using the experimental parameters and four protons with the hfc value as indicated in Table 2.

For EPR measurements at 10 K, a closed-cycle cryostat (Cryogenic CF VTC) in a helium atmosphere was used for temperature control. Pulsed optical excitation at 10 K was provided by a Nd:YAG laser (Spectra-Physics Quanta-Ray INDI PS 51/52) equipped with a second harmonic module, a pulse width of approximately 6 ns, a pulse energy of 3–5 mJ and a shot repetition rate of 20 Hz.

X-Band TREPR experiments at 10 K were performed on an Elexsys E580 X-Band Pulse Spectrometer system and a dielectric-ring resonator (Bruker ER 4118X-MD5). Q-Band EPR measurements at 10 K were performed on a Bruker Elexsys E580 Super Q-FT spectrometer equipped with a EN5107D2 resonator. Q-band ENDOR measurements were performed applying the Davies ENDOR sequence laser-DAF-($\pi$)-($\pi_{rf}$)-($\pi/2$)-$t$-($\pi$). The DAF was 500 ns, delay $t$ was set to 400 ns. 40 ns long gaussian-shaped pulses with different amplitudes were employed along with an 11 μs RF pulse amplified using a Bruker 250 W RF amplifier. The values of the proton hfcs along the principal axes of the ZFS tensor were determined by Gaussian deconvolution of the ENDOR spectra.

### 4.3. TREPR simulations

The simulation of the time evolution of the magnetization after its generation by population of the molecular triplet state of **AlOEP** by intersystem crossing was performed by solving the master equation reported in Refs. [42,43]. The master equation accounts for the decay to the ground state of the triplet, the spin lattice relaxation time and the reaching of the Boltzmann population distribution between levels in the absence of decay processes. For each field position, the on-resonance/off-resonance contributions were calculated by the appropriate integration over the possible relative orientations of the triplet molecule and of the external magnetic field as

$$I(B_0,t)=\sum\nolimits_{\pm}\iint G[B_{res\pm}(\vartheta,\varphi)-B_0]\cdot\Delta P_{\pm}(\vartheta,\varphi,t)sin\vartheta d\vartheta d\varphi \qquad (2)$$

where $G[B_{res\pm}(\vartheta,\varphi)-B_0]$ is a line shape function, $B_{res}$ is the resonance field at a given orientation $(\vartheta,\varphi)$ of the magnetic field $B_0$, and $\Delta P_{\pm}(\vartheta,\varphi,t)$ is the non-Boltzmann population differences between the two resonant states. The resonance fields were calculated upon diagonalization of the Hamiltonian $H=\mu_B\boldsymbol{S}\cdot\boldsymbol{g}\cdot\boldsymbol{B}_0+\mathbf{S}\cdot\mathbf{D}\cdot\mathbf{S}$, where **D** is the dipolar tensor. The calculation was performed by programming Eq. (2) in MATLAB™ and using a least square fitting routine to fit the signal intensity to the experimental dataset.

### 4.4. DFT calculations

The hfcs for **AlOEP** were calculated using ORCA 5.0.2 [65,66]. The structure was first constructed using the program Avogadro [67] from the X-ray crystal structure data of a related porphyrin [68] and then subjected to energy minimization using the UFF force field either with or without a coordinated MeTHF molecule [69]. The geometry of the triplet state was then optimized in ORCA using the PBE functional [70] and the def2-TZVP basis set [71] with the D3 dispersion correction [72]. The resolution of identity approximation [73] was used to speed up the calculations. A single point calculation was then performed using the EPRNMR module of Orca to determine the hfcs. The obtained hyperfine tensors were rotated into the ZFS principal axis frame obtained from CASSCF computations the details of which are described elsewhere [12].

## Data availability

All data are available in the manuscript or in the Supporting Information

## Declaration of Competing Interest

The authors declare that they have no known competing financial interests or personal relationships that could have appeared to influence the work reported in this paper.

## Acknowledgements

S.C., A.B. and M.D.V. gratefully acknowledge the Interdepartmental Centre Giorgio Levi Cases for Energy Economics and Technology (Biomolecular DSSCs Project) for financial support. A.C. would like to thank Department of Chemical Sciences of the University of Padua for a Nexus project scholarship and Prof. C. W. M. Kay for the opportunity to work at Saarland University. AvdE acknowledges support from NSERC (Discovery Grant 2015-04021). This work was made possible by the facilities of the Shared Hierarchical Academic Research Computing Network (SHARCNET:www.sharcnet.ca) and Compute/Calcul Canada. This work was supported by the Chancellor's Faculty Small Grant - University of Minnesota Duluth to PKP. EPR spectroscopy at Saarland University was performed on spectrometers purchased with support of the State of Saarland and the German Science Foundation (project number INST256/535-1).

## Appendix A. Supplementary material

Supplementary material to this article can be found online at https://doi.org/10.1016/j.jmr.2023.107515.

## References

[1] N. Zarrabi, P.K. Poddutoori, Aluminum(III) porphyrin: A unique building block for artificial photosynthetic systems, Coord. Chem. Rev. 429 (2021), https://doi.org/10.1016/j.ccr.2020.213561.
[2] E. Nikoloudakis, I. López-Duarte, G. Charalambidis, K. Ladomenou, M. Ince, A.G. Coutsolelos, Porphyrins and phthalocyanines as biomimetic tools for photocatalytic $H_2$ production and $CO_2$ reduction, Chem. Soc. Rev. 51 (2022) 6965–7045, https://doi.org/10.1039/D2CS00183G.
[3] S. Fukuzumi, Y.-M. Lee, W. Nam, Bioinspired artificial photosynthesis systems, Tetrahedron 76 (2020), https://doi.org/10.1016/j.tet.2020.131024.
[4] M. Borgström, E. Blart, G. Boschloo, E. Mukhtar, A. Hagfeldt, L. Hammarström, F. Odobel, Sensitized Hole Injection of Phosphorus Porphyrin into NiO: Toward New Photovoltaic Devices, J. Phys. Chem. B. 109 (2005) 22928–22934, https://doi.org/10.1021/jp054034a.
[5] P.K. Poddutoori, J.M. Thomsen, R.L. Milot, S.W. Sheehan, C.F.A. Negre, V.K.R. Garapati, C.A. Schmuttenmaer, V.S. Batista, G.W. Brudvig, A. van der Est, Interfacial electron transfer in photoanodes based on phosphorus(V) porphyrin sensitizers co-deposited on $SnO_2$ with the Ir(III)Cp* water oxidation precatalyst, J. Mater. Chem. A. 3 (2015) 3868–3879, https://doi.org/10.1039/C4TA07018F.
[6] P. Zwick, D. Dulić, H.S.J. van der Zant, M. Mayor, Porphyrins as building blocks for single-molecule devices, Nanoscale 13 (2021) 15500–15525, https://doi.org/10.1039/D1NR04523G.
[7] D. Dini, M.J.F. Calvete, M. Hanack, Nonlinear Optical Materials for the Smart Filtering of Optical Radiation, Chem. Rev. 116 (2016) 13043–13233, https://doi.org/10.1021/acs.chemrev.6b00033.
[8] F. Leng, H. Liu, M. Ding, Q.-P. Lin, H.-L. Jiang, Boosting Photocatalytic Hydrogen Production of Porphyrinic MOFs: The Metal Location in Metalloporphyrin Matters, ACS Catal. 8 (2018) 4583–4590, https://doi.org/10.1021/acscatal.8b00764.
[9] J. Jiang, K.L. Materna, S. Hedström, K.R. Yang, R.H. Crabtree, V.S. Batista, G.W. Brudvig, Antimony Complexes for Electrocatalysis: Activity of a Main-Group Element in Proton Reduction, Angew. Chem. Int. Ed. 56 (2017) 9111–9115, https://doi.org/10.1002/anie.201704700.
[10] P. Agostinis, K. Berg, K.A. Cengel, T.H. Foster, A.W. Girotti, S.O. Gollnick, S.M. Hahn, M.R. Hamblin, A. Juzeniene, D. Kessel, M. Korbelik, J. Moan, P. Mroz, D. Nowis, J. Piette, B.C. Wilson, J. Golab, Photodynamic therapy of cancer: An update, CA Cancer J. Clin. 61 (2011) 250–281, https://doi.org/10.3322/caac.20114.

[11] N. Zarrabi, B.J. Bayard, S. Seetharaman, N. Holzer, P. Karr, S. Ciuti, A. Barbon, M. Di Valentin, A. Van Der Est, F. D'Souza, P.K. Poddutoori, A charge transfer state induced by strong exciton coupling in a cofacial μ-oxo-bridged porphyrin heterodimer, Phys. Chem. Chem. Phys. 23 (2021) 960–970, https://doi.org/10.1039/d0cp05783e.

[12] S. Ciuti, J. Toninato, A. Barbon, N. Zarrabi, P.K. Poddutoori, A. van der Est, M. Di Valentin, Solvent dependent triplet state delocalization in a co-facial porphyrin heterodimer, Phys. Chem. Chem. Phys. 24 (2022) 30051–30061, https://doi.org/10.1039/D2CP04291F.

[13] W. Lubitz, Pulse EPR and ENDOR studies of light-induced radicals and triplet states in photosystem II of oxygenic photosynthesis, Phys. Chem. Chem. Phys. 4 (2002) 5539–5545, https://doi.org/10.1039/B206551G.

[14] W. Lubitz, F. Lendzian, R. Bittl, Radicals, Radical Pairs and Triplet States in Photosynthesis, Acc. Chem. Res. 35 (2002) 313–320, https://doi.org/10.1021/ar000084g.

[15] S. Richert, C.E. Tait, C.R. Timmel, Delocalisation of photoexcited triplet states probed by transient EPR and hyperfine spectroscopy, J. Magn. Reson. 280 (2017) 103–116, https://doi.org/10.1016/j.jmr.2017.01.005.

[16] S. Weber, EPR Transient, EMagRes, John Wiley & Sons, Ltd, 2017, pp. 255–270, https://doi.org/10.1002/9780470034590.emrstm1509.

[17] C.E. Tait, M.D. Krzyaniak, S. Stoll, Computational tools for the simulation and analysis of spin-polarized EPR spectra, J. Magn. Reson. 349 (2023), https://doi.org/10.1016/j.jmr.2023.107410.

[18] T.S. Lin, Electron spin echo spectroscopy of organic triplets, Chem. Rev. 84 (1984) 1–15, https://doi.org/10.1021/cr00059a001.

[19] M. Di Valentin, S. Ceola, E. Salvadori, G. Agostini, G.M. Giacometti, D. Carbonera, Spectroscopic properties of the peridinins involved in chlorophyll triplet quenching in high-salt peridinin–chlorophyll *a*-protein from Amphidinium carterae as revealed by optically detected magnetic resonance, pulse EPR and pulse ENDOR spectroscopies, Biochimica et Biophysica Acta (BBA) – Bioenergetics 1777 (2008) 1355–1363, https://doi.org/10.1016/j.bbabio.2008.06.006.

[20] A. Toffoletti, Z. Wang, J. Zhao, M. Tommasini, A. Barbon, Precise determination of the orientation of the transition dipole moment in a Bodipy derivative by analysis of the magnetophotoselection effect, Phys. Chem. Chem. Phys. 20 (2018) 20497–20503, https://doi.org/10.1039/c8cp01984c.

[21] A. Barbon, M.G. Dal Farra, S. Ciuti, M. Albertini, L. Bolzonello, L. Orian, M. Di Valentin, Comprehensive investigation of the triplet state electronic structure of free-base 5,10,15,20-tetrakis(4-sulfonatophenyl)porphyrin by a combined advanced EPR and theoretical approach, J. Chem. Phys. 152 (2020), https://doi.org/10.1063/1.5131753.

[22] S. Ciuti, A. Carella, A. Lucotti, M. Tommasini, A. Barbon, M. Di Valentin, Insights into the phototautomerism of free-base 5, 10, 15, 20-tetrakis(4-sulfonatophenyl) porphyrin, Photochem. Photobiol. Sci. (2023), https://doi.org/10.1007/s43630-023-00413-5.

[23] M.D. Kemple, ENDOR of Triplet State Systems in Solids, in: M.M. Dorio, J.H. Freed (Eds.), Multiple Electron Resonance Spectroscopy, Springer US, Boston, MA, 1979, pp. 409–436. https://doi.org/10.1007/978-1-4684-3441-5_12

[24] C. Gemperle, A. Schweiger, Pulsed electron-nuclear double resonance methodology, Chem. Rev. 91 (1991) 1481–1505, https://doi.org/10.1021/cr00007a011.

[25] K. Möbius, A. Savitsky, High-Field EPR Spectroscopy on Proteins and their Model Systems: Characterization of Transient Paramagnetic States, R. Soc. Chem. (2008), https://doi.org/10.1039/9781847559272.

[26] L. Kulik, W. Lubitz, Electron-nuclear double resonance, Photosynth. Res. 102 (2009) 391–401, https://doi.org/10.1007/s11120-009-9401-y.

[27] J.R. Harmer, Hyperfine spectroscopy-ENDOR, EMagRes 5 (2016) 1493–1514, https://doi.org/10.1002/9780470034590.emrstm1515.

[28] J. Niklas, A. Agostini, D. Carbonera, M. Di Valentin, W. Lubitz, Primary donor triplet states of Photosystem I and II studied by Q-band pulse ENDOR spectroscopy, Photosynth. Res. 152 (2022) 213–234, https://doi.org/10.1007/s11120-022-00905-y.

[29] M. Di Valentin, C.E. Tait, E. Salvadori, L. Orian, A. Polimeno, D. Carbonera, Evidence for water-mediated triplet–triplet energy transfer in the photoprotective site of the peridinin–chlorophyll a–protein, Biochimica et Biophysica Acta (BBA) – Bioenergetics 1837 (2014) 85–97, https://doi.org/10.1016/j.bbabio.2013.07.005.

[30] J.H. van der Waals, W.G. van Dorp, T.J. Schaafsma, Electron spin resonance of porphyrin excited states, in: The Porphyrins, Vol. IV, Academic Press, 1979, pp. 257–312. https://research.wur.nl/en/publications/electron-spin-resonance-of-porphyrin-excited-states (accessed June 10, 2023).

[31] S.R. Langhoff, E.R. Davidson, M. Gouterman, W.R. Leenstra, A.L. Kwiram, Zero field splitting of the triplet state of porphyrins. II, J. Chem. Phys. 62 (2008) 169–176, https://doi.org/10.1063/1.430249.

[32] M. Gouterman, Angular Momentum, Magnetic Interactions, Jahn-Teller and Environment Effects in Metalloporphyrin Triplet States, Ann. N. Y. Acad. Sci. 206 (1973) 70–83, https://doi.org/10.1111/j.1749-6632.1973.tb43205.x.

[33] P.J. Angiolillo, J.M. Vanderkooi, Electron paramagnetic resonance of the excited triplet state of metal-free and metal-substituted cytochrome c | Elsevier Enhanced Reader, (n.d.). https://doi.org/10.1016/S0006-3495(95)80433-9.

[34] B.M. Hoffman, M.A. Ratner, Jahn-Teller effects in metalloporphyrins and other four-fold symmetric systems, (n.d.), Mol. Phys. 35 (1978) 901–925, https://doi.org/10.1080/00268977800100671.

[35] K.A. Nguyen, R. Pachter, Jahn-Teller triplet excited state structures and spectra of zinc complexes of porphyrin and phthalocyanine: A density functional theory study, J. Chem. Phys. 118 (2003) 5802–5810, https://doi.org/10.1063/1.1540627.

[36] P.J. Angiolillo, J.M. Vanderkooi, The Photoexcited Triplet State as a Probe of Chromophore-Protein Interaction in Myoglobin, Biophys. J. 75 (1998) 1491–1502, https://doi.org/10.1016/S0006-3495(98)74068-8.

[37] P.J. Angiolillo, V.-S.-Y. Lin, J.M. Vanderkooi, M.J. Therien, EPR Spectroscopy and Photophysics of the Lowest Photoactivated Triplet State of a Series of Highly Conjugated (Porphinato)Zn Arrays, J. Am. Chem. Soc. 117 (1995) 12514–12527, https://doi.org/10.1021/ja00155a015.

[38] M.G.D. Farra, C. Martin, E. Bergantino, Y.E. Kandrashkin, A. van der Est, M. Di Valentin, Electron spin polarization transfer induced by triplet–radical interactions in the weakly coupled regime, Phys. Chem. Chem. Phys. 22 (2020) 19982–19991, https://doi.org/10.1039/D0CP03565C.

[39] Y.E. Kandrashkin, M. Di Valentin, A. van der Est, Reversible triplet energy hopping in photo-excited molecules: A two-site model for the spin polarization, J. Chem. Phys. 153 (2020), https://doi.org/10.1063/5.0022164.

[40] S. Ciuti, A. Barbon, M. Bortolus, A. Agostini, E. Bergantino, C. Martin, M. Di Valentin, D. Carbonera, Neuroglobin Provides a Convenient Scaffold to Investigate the Triplet-State Properties of Porphyrins by Time-Resolved EPR Spectroscopy and Magnetophotoselection, Appl. Magn. Reson. 53 (2022) 1031–1042, https://doi.org/10.1007/s00723-021-01421-3.

[41] R. Furrer, P. Fujara, C. Lange, D. Stehlik, H.M. Vieth, W. Vollmann, Transient ESR nutation signals in excited aromatic triplet states, Chem. Phys. Lett. 75 (1980) 332–339, https://doi.org/10.1016/0009-2614(80)80526-4.

[42] Z. Wang, A. Toffoletti, Y. Hou, J. Zhao, A. Barbon, B. Dick, Insight into the drastically different triplet lifetimes of BODIPY obtained by optical/magnetic spectroscopy and theoretical computations, Chem. Sci. 12 (2021) 2829–2840, https://doi.org/10.1039/D0SC05494A.

[43] C.J. Winscom, Analysis of Spin Polarisation Transients in Periodically Photo-excited Triplet States, Zeitschrift Für Naturforschung A 30 (1975) 571–582, https://doi.org/10.1515/zna-1975-0501.

[44] P.J.F. Verbeek, A.I.M. Dicker, J. Schmidt, Spin—lattice relaxation processes in photo-excited triplet states through a rotation of the spin axes on thermal excitation, Chem. Phys. Lett. 56 (1978) 585–590, https://doi.org/10.1016/0009-2614(78)89047-2.

[45] B.M. Hoffman, V.J. DeRose, P.E. Doan, R.J. Gurbiel, A.L.P. Houseman, J. Telser, Metalloenzyme Active-Site Structure and Function through Multifrequency CW and Pulsed ENDOR, in: L.J. Berliner, J. Reuben (Eds.), EMR of Paramagnetic Molecules, Springer US, Boston, MA, 1993, pp. 151–218, https://doi.org/10.1007/978-1-4615-2892-0_4.

[46] A. Agostini, D.M. Palm, F.-J. Schmitt, M. Albertini, M. Di Valentin, H. Paulsen, D. Carbonera, An unusual role for the phytyl chains in the photoprotection of the chlorophylls bound to Water-Soluble Chlorophyll-binding Proteins, Sci. Rep. 7 (2017) 7504, https://doi.org/10.1038/s41598-017-07874-6.

[47] C.E. Tait, P. Neuhaus, H.L. Anderson, C.R. Timmel, Triplet State Delocalization in a Conjugated Porphyrin Dimer Probed by Transient Electron Paramagnetic Resonance Techniques, J. Am. Chem. Soc. 137 (2015) 6670–6679, https://doi.org/10.1021/jacs.5b03249.

[48] C.E. Tait, P. Neuhaus, H.L. Anderson, C.R. Timmel, D. Carbonera, M. Di Valentin, HYSCORE on Photoexcited Triplet States, Appl. Magn. Reson. 46 (2015) 389–409, https://doi.org/10.1007/s00723-014-0624-5.

[49] R. Quinn, J.S. Valentine, M.P. Byrn, C.E. Strouse, Electronic structure of low-spin ferric porphyrins: a single-crystal EPR and structural investigation of the influence of axial ligand orientation and the effects of pseudo-Jahn-Teller distortion, J. Am. Chem. Soc. 109 (1987) 3301–3308, https://doi.org/10.1021/ja00245a019.

[50] S.K. Hoffmann, J. Goslar, W. Hilczer, M.A. Augustyniak, M. Marciniak, Vibronic Behavior and Electron Spin Relaxation of Jahn−Teller Complex $Cu(H_2O)_6^{2+}$ in $(NH_4)_2Mg(SO_4)_2{\cdot}6H_2O$ Single Crystal, J. Phys. Chem. A 102 (1998) 1697–1707, https://doi.org/10.1021/jp971834f.

[51] S.K. Hoffmann, J. Goslar, W. Hilczer, R. Kaszyński, M.A. Augustyniak-Jabłokow, Electron spin relaxation of the Jahn-Teller $Cu(H_2O)_6$ complex in $Cs_2Zn(SO_4)_2{\cdot}6H_2O$ crystals, Solid State Commun. 117 (2001) 333–336, https://doi.org/10.1016/S0038-1098(00)00464-6.

[52] B.L. Silver, D. Getz, ESR of $Cu^{2+}(H_2O)_6$. II. A quantitative study of the dynamic Jahn-Teller effect in copper-doped zinc Tutton's salt, J. Chem. Phys. 61 (1974) 638–650, https://doi.org/10.1063/1.1681940.

[53] M.J. Riley, M.A. Hitchman, A.W. Mohammed, Interpretation of the temperature dependent g values of the $Cu(H_2O)_6^{2+}$ ion in several host lattices using a dynamic vibronic coupling model, J. Chem. Phys. 87 (1987) 3766–3778, https://doi.org/10.1063/1.452932.

[54] S. Kiczka, S.K. Hoffmann, J. Goslar, L. Szczepanska, Electronic structure, Jahn-Teller dynamics and electron spin relaxation of two types of octahedral Cu(II) complexes in cadmium formate dihydrate $Cd(HCOO)_2{\cdot}2H_2O$. EPR and ESE studies, Phys. Chem. Chem. Phys. 6 (2004) 64–71, https://doi.org/10.1039/B311063J.

[55] W.G. van Dorp, M. Soma, J.A. Kooter, J.H. van der Waals, Electron spin resonance in the photo-excited triplet state of free base porphin in a single crystal of n-octane, Mol. Phys. 28 (1974) 1551–1568, https://doi.org/10.1080/00268977400102801.

[56] C.W.M. Kay, The Electronic Structure of the Photoexcited Triplet State of Free-Base (Tetraphenyl)porphyrin by Time-Resolved Electron-Nuclear Double Resonance and Density Functional Theory, J. Am. Chem. Soc. 125 (2003) 13861–13867, https://doi.org/10.1021/ja036278j.

[57] C.W.M. Kay, M. Di Valentin, K. Möbius, A time-resolved Electron Nuclear Double Resonance (ENDOR) study of the photoexcited triplet state of free-base

tetraphenylporphyrin, Sol. Energy Mater. Sol. Cells 38 (1995) 111–118, https://doi.org/10.1016/0927-0248(94)00219-3.
[58] V. Hamacher, J. Wrachtrap, B. von Maltzan, M. Plato, K. Möbius, EPR and ENDOR study of porphyrins and their covalently linked dimers in the photoexcited triplet state, Appl. Magn. Reson. 4 (1993) 297–319, https://doi.org/10.1007/BF03162504.
[59] C.E. Tait, P. Neuhaus, M.D. Peeks, H.L. Anderson, C.R. Timmel, Transient EPR Reveals Triplet State Delocalization in a Series of Cyclic and Linear π-Conjugated Porphyrin Oligomers, J. Am. Chem. Soc. 137 (2015) 8284–8293, https://doi.org/10.1021/jacs.5b04511.
[60] A.J. Redman, G. Moise, S. Richert, E.J. Viere, W.K. Myers, M.J. Therien, C.R. Timmel, EPR of Photoexcited Triplet-State Acceptor Porphyrins, J. Phys. Chem. C 125 (2021) 11782–11790, https://doi.org/10.1021/acs.jpcc.1c03278.
[61] M. Di Valentin, M. Albertini, E. Zurlo, M. Gobbo, D. Carbonera, Porphyrin Triplet State as a Potential Spin Label for Nanometer Distance Measurements by PELDOR Spectroscopy, J. Am. Chem. Soc. 136 (2014) 6582–6585, https://doi.org/10.1021/ja502615n.
[62] M. Di Valentin, M. Albertini, M.G. Dal Farra, E. Zurlo, L. Orian, A. Polimeno, M. Gobbo, D. Carbonera, Light-Induced Porphyrin-Based Spectroscopic Ruler for Nanometer Distance Measurements, Chem. – Eur. J. 22 (2016) 17204–17214, https://doi.org/10.1002/chem.201603666.
[63] A. Bertran, K.B. Henbest, M. De Zotti, M. Gobbo, C.R. Timmel, M. Di Valentin, A. M. Bowen, Light-Induced Triplet-Triplet Electron Resonance Spectroscopy, J. Phys. Chem. Lett. 12 (2021) 80–85, https://doi.org/10.1021/acs.jpclett.0c02884.
[64] S. Stoll, A. Schweiger, EasySpin, a comprehensive software package for spectral simulation and analysis in EPR, J. Magn. Reson. 178 (2006) 42–55, https://doi.org/10.1016/j.jmr.2005.08.013.
[65] F. Neese, The ORCA program system, WIREs Comput. Mol. Sci. 2 (2012) 73–78, https://doi.org/10.1002/wcms.81.
[66] F. Neese, Software update: the ORCA program system, version 4.0, WIREs Comput. Mol. Sci. 8 (2018) e1327, https://doi.org/10.1002/wcms.1327.
[67] M.D. Hanwell, D.E. Curtis, D.C. Lonie, T. Vandermeersch, E. Zurek, G.R. Hutchison, Avogadro: an advanced semantic chemical editor, visualization, and analysis platform, J. Cheminf. 4 (2012) 17, https://doi.org/10.1186/1758-2946-4-17.
[68] R. Guilard, A. Zrineh, A. Tabard, A. Endo, B.C. Han, C. Lecomte, M. Souhassou, A. Habbou, M. Ferhat, K.M. Kadish, Synthesis and spectroscopic and electrochemical characterization of ionic and.sigma.-bonded aluminum(III) porphyrins. Crystal structure of methyl(2,3,7,8,12,13,17,18-octaethylporphinato)aluminum(III), (OEP)Al(CH3), Inorg. Chem. 29 (1990) 4476–4482, https://doi.org/10.1021/ic00347a029.
[69] A.K. Rappe, C.J. Casewit, K.S. Colwell, W.A. Goddard, W.M. Skiff, UFF, a full periodic table force field for molecular mechanics and molecular dynamics simulations, J. Am. Chem. Soc. 114 (1992) 10024–10035, https://doi.org/10.1021/ja00051a040.
[70] J.P. Perdew, K. Burke, M. Ernzerhof, Generalized Gradient Approximation Made Simple, Phys. Rev. Lett. 77 (1996) 3865–3868, https://doi.org/10.1103/PhysRevLett.77.3865.
[71] F. Weigend, R. Ahlrichs, Balanced basis sets of split valence, triple zeta valence and quadruple zeta valence quality for H to Rn: Design and assessment of accuracy, Phys. Chem. Chem. Phys. 7 (2005) 3297, https://doi.org/10.1039/b508541a.
[72] S. Grimme, J. Antony, S. Ehrlich, H. Krieg, A consistent and accurate *ab initio* parametrization of density functional dispersion correction (DFT-D) for the 94 elements H-Pu, J. Chem. Phys. 132 (2010), https://doi.org/10.1063/1.3382344.
[73] R.A. Kendall, H.A. Früchtl, The impact of the resolution of the identity approximate integral method on modern ab initio algorithm development, Theor. Chem. Acta 97 (1997) 158–163, https://doi.org/10.1007/s002140050249.